Chemistry–A European Journal
Research Article
doi.org/10.1002/chem.202201959
Chemistry Europe
European Chemical Societies Publishing
www.chemeurj.org

Elastin-Hyaluronan Bioconjugate as Bioactive Component in Electrospun Scaffolds

Antonio Laezza,[a] Antonietta Pepe,[a] and Brigida Bochicchio*[a]

Abstract: Hyaluronic acid or hyaluronan (HA) and elastin-inspired peptides (EL) have been widely recognized as bioinspired materials useful in biomedical applications. The aim of the present work is the production of electrospun scaffolds as wound dressing materials which would benefit from synergic action of the bioactivity of elastin peptides and the regenerative properties of hyaluronic acid. Taking advantage of thiol-ene chemistry, a bioactive elastin peptide was successfully conjugated to methacrylated hyaluronic acid (MAHA) and electrospun together with poly-D,L-lactide (PDLLA). To the best of our knowledge, limited reports on peptide-conjugated hyaluronic acid were described in literature, and none of these was employed for the production of electrospun scaffolds. The conformational studies carried out by Circular Dichroism (CD) on the bioconjugated compound confirmed the preservation of secondary structure of the peptide after conjugation while Scanning Electron Microscopy (SEM) revealed the supramolecular structure of the electrospun scaffolds. Overall, the study demonstrates that the bioconjugation of hyaluronic acid with the elastin peptide improved the electrospinning processability with improved characteristics in terms of morphology of the final scaffolds.

Introduction

Elastic fibres confer resilience and elastic recoil to organs and tissues as lung, skin, and blood vessels. They are present in the extracellular matrix (ECM) of vertebrates and are composed of two distinct morphological entities. The amorphous component is made up of elastin which is a crosslinked and insoluble protein assembled from a soluble precursor called tropoelastin. The microfibrillar component is composed of glycoproteins, as fibrillin-1 and fibrillin-2, and acts as three-dimensional scaffold for the assembly of elastin.[1] The ordered organization of elastic fibres is functional to elastin mechanical properties and it is definitely lost after injury, as elastin turnover is almost absent in adults.[2] Therefore, during wound healing the low level of elastin production entails the formation of scars with poor elasticity. Since elastogenesis is an age-decreasing process, the development of dressings based on elastin peptides able to promote attachment, spreading, proliferation, and differentiation of fibroblasts, smooth muscle, and endothelial cells has raised increased interest over years.[3] Electrospinning is able to produce fibres in the sub-micrometer range giving rise to matrices characterised by the presence of pores and high surface to volume ratios, properties which favour cellular growth.[4] This technique has been deeply employed with different polymers[5] as poly(glycolic) acid (PGA), poly(lactic-acid) (PLA), and their copolymer, poly (lacto-co-glycolic acid) (PLGA),[6] polycaprolactone (PCL),[7] poly(vinyl-alcohol) (PVA),[8] poly(ethylene-glycol) (PEO), and poly(vinyl-pyrrolidone) (PVP). In the last decades, recombinant tropoelastin-based electrospun scaffolds were produced as wound dressing matrices able to mimic the architecture of ECM.[9] Recently, we have obtained electrospun scaffolds by co-electrospinning and blending elastin-derived peptides with other natural or synthetic materials, such as gelatin, poly-D,L-lactide and nanocellulose crystals (CNCs).[10] Besides, the natural polymer HA has been widely used in biomaterial synthesis.[11] HA is a non-sulfated polysaccharide composed of D-glucuronic acid (GlcA) and *N*-acetyl-D-glucosamine (GlcNAc), linked by alternating β-1→3 and β-1→4 glycosidic bonds, resulting in 4)-β-GlcA-(1→3)-β-GlcNAc-(1→ disaccharide repeating units. It is part of glycosaminoglycans (GAGs), a class of linear anionic heteropolysaccharides that are ubiquitously found in ECM.[12] Hyaluronic acid plays important roles in wound healing by influencing inflammation, cell migration and proliferation, angiogenesis, and re-epithelialization processes,[13] rendering HA useful for biomedical applications as, for example, wound dressing. The advantages in the use of HA, besides the biocompatibility and the biodegradability, are represented by the functional groups on polysaccharide backbone enabling its employment in wound dressing. Hydroxyl and carboxyl groups, for example, confer to the glycosaminoglycan a high degree of hydrophilicity that promote cellular adhesion and enable exudates absorption,[14] beyond permitting the chemical functionalization of the backbone useful for obtaining tailored derivatives. Despite its numerous advantages, the electrospinnability of HA shows

[a] *Dr. A. Laezza, Prof. A. Pepe, Prof. B. Bochicchio*
Department of Science
University of Basilicata
Viale dell'Ateneo Lucano 10, 85100, Potenza (Italy)http://docenti.unibas.it/site/home/docente.html?m=003216
E-mail: brigida.bochicchio@unibas.it

Supporting information for this article is available on the WWW under https://doi.org/10.1002/chem.202201959

some difficulties. One of the major problems occurring when HA is electrospun is represented by the high viscosity of concentrated solutions, which becomes even more critical in aqueous solution due to the ionic nature of polysaccharide promoting long-range electrostatic interactions. High viscosities do not guarantee the adequate interlocking of polymer chains, causing electrospinning with unstable jets and, consequently, the formation of membranes with heterogeneous and discontinuous nanofibers. Decreasing the viscosity and surface tension of polymeric solutions by blending HA with other polymers and by using organic solvents for electrospinning were the main solutions proposed to work around this problem.[7,15] Alternatively, hybrid gelatin-poly-L-lactide blends were electrospun in 1,1,1,3,3,3-Hexafluoro-2-propanol (HFP) and subsequently crosslinked with HA.[16] Recently, the chemical modification of HA represented another alternative not only aimed to improve the processability of the GAG by electrospinning but also to prolong its degradation time.[17] To the best of our knowledge, limited reports on peptide-conjugated hyaluronic acid were described in literature, and none of these was employed for the production of electrospun scaffolds. Otherwise, graft polymers of HA were synthetized and not electrospun.[18]

Literature data show that the bioconjugation of HA with polymers was carried out by taking advantage of hydroxyl and carboxyl groups of the polysaccharide. Different strategies have been developed for HA modification to ameliorate its biological applications. Recently, the glycosaminoglycan has been conjugated with a hydrazine-modified elastin peptide after an oxidative cleavage of the backbone, which converted secondary hydroxyl groups of GlcA into aldehydes.[19] Other approaches include the insertion of methacrylate pending moiety exploiting either carboxyl or hydroxyls reactivity to obtain photocrosslinkable HA hydrogels as biomaterials biologically improved for tissue regeneration applications.[20] Concerning carboxyl group, the transformation into active ester by reaction with carbodiimide/HOBT was a successful strategy for coupling different amine groups to HA which could be useful for carrying out coupling or crosslinking reactions under mild physiological conditions.[21]

Taking advantage of previous experience in conjugating peptides to carbohydrates,[22] in this work we have synthesised an elastin-hyaluronan bioconjugate (ELHA). The methacrylated hyaluronic acid has been covalently conjugated using thiol-Michael coupling reaction[23] to a 21-residues conjugated elastin-derived peptide containing a N-terminal cysteine. The peptide sequence is (C)AAAAAAAAAAKAAKYGAAAGL (EL) and corresponds to the region 302–322 of human tropoelastin (HTE) promoting cell attachment and spreading.[24] ELHA was studied at molecular level by CD and Attenuated Total Reflectance Fourier Transform Infrared Spectroscopy (ATR-FTIR) and then electrospun with racemic PDLLA. Finally, the morphology of electrospun scaffolds was investigated by SEM with the perspective of applications as wound dressing materials.

Results and Discussion

Synthesis of elastin glycoconjugate

The strategy to obtain elastin-hyaluronan glycoconjugate by thiol Michael-type addition started with the synthesis of **1** (EL) by solid-phase peptide synthesis (SPPS) (Scheme 1). The peptide is alanine-rich and is prone to self-aggregation,[25] in order to avoid this drawback a low loading resin (0.34 mmol/g) was used. The main risk of incorporating cysteine on the chain during SPPS consists of high propensity to racemization under standard coupling conditions.[26] Therefore, to limit this undesired side effect the activation time of cysteine coupling was reduced from 2.0 to 1.0 minutes. Finally, the peptide was obtained after resin-peptide detachment in 87% mass yield. High-Performance Liquid Chromatography (HPLC) analysis afforded the peptide with 97% purity (Figure S1). The molecular weight of the peptide was assessed by Matrix-Assisted Laser Desorption/Ionization-Time of Flight (MALDI-TOF) mass spectrum (Figure S2) showing a peak at m/z: 1874.9 $[M+H]^+$ according to the expected MW of 1873.9 for the synthesized peptide. The peptide sequence was confirmed by ^{1}H NMR spectrum (Figure S3).

GlcA unit of sodium hyaluronate was amidated at the carboxyl group by the insertion of methacrylate moiety for functionalizing the polysaccharide with peptide **1**. Typically, the amide bond is formed by activating the carboxylic acid with phosphonium and uronium/guanidinium salts, carbodiimides, and triazines.[27]

Several studies have been conducted both on unsulphated[28] and sulphated glycosaminoglycans.[29]

The decoration of HA with methacrylate linker was accomplished in water in the presence of 2-aminoethyl methacrylate hydrochloride (2-AEMA·HCl), *N*-(3-(dimethylamino)propyl)-*N'*-ethylcarbodiimide reagent (EDC) and *N*-hydroxysulfosuccinimide (NHS) at pH = 6.8, (Scheme 2, a). After overnight reaction at room temperature, dialysis and subsequent freeze-drying furnished MAHA polysaccharide **2** in 98% mass yield and with a degree of substitution (DS) of 0.18, as calculated by ^{1}H NMR.

^{1}H NMR spectrum of MAHA **2** confirmed the amide bond formation with 2-AEMA for the presence of signals at δ_{DSS} = 1.91 ppm, δ_{DSS} = 4.23 ppm, δ_{DSS} = 5.73 ppm, and δ_{DSS} = 6.14 ppm, respectively associated to the to $-CH_3$, $-OCH_2-$, and $=CH_2$ groups, of methacrylate linker (Figure 1, red). The DS of derivative **2** was calculated by comparing the ^{1}H NMR vinyl (δ_{DSS} = 5.73, or 6.14 ppm) integrals with that obtained by the

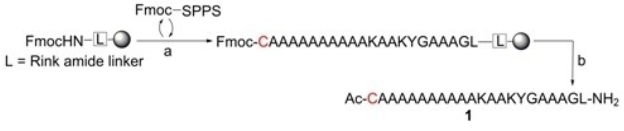

Scheme 1. Fmoc-SPPS synthesis of peptide **1**. (a) i) 20% Piperidine, DMF, RT; ii) Fmoc-AA:HBTU:HOBT:DIPEA, 5:5:5:10, RT, DMF, temperature; iii) Ac_2O, DIPEA, DMF, RT; (b) i) 20% Piperidine, DMF, RT; ii) Ac_2O, DIPEA, DMF, RT; iii) 94% TFA, 2.5% EDT, 2.5% H_2O, 1% TIS, RT, 1.5 h, yield 87%.

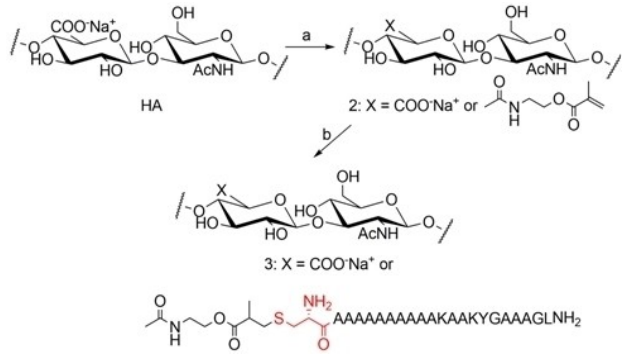

Scheme 2. Semi-synthesis of polysaccharide 3 . (a) 2-AEMA·HCl, EDC, s-NHS, H_2O, RT, pH = 6.8, overnight, yield 98%, DS = 0.18; (b) **1**, TCEP·HCl, H_2O, RT, pH = 8.9, 2d, yield = 67%, DS = 1.0.

sum of HA and 2-AEMA acetyl signals (δ_{DSS} = 2.01 and 1.91 ppm) (Figure S4) by Equation (1):

$$DS = \frac{3I_{CH(AEMA)}}{I_{CH_3(GlcNAc)+CH_3(AEMA)} - 3I_{CH\ (AEMA)}} 100 \quad (1)$$

where $I_{CH(AEMA)}$ represents the proton integral of the AEMA methine proton, while $I_{CH3(GlcNAc)}$ and $I_{CH3(AEMA)}$ represent the proton integrals of the methyl groups of GlcNAc and AEMA, respectively.

Product **2** was coupled to the cysteine thiol at *N*-terminal residue of EL peptide **1** via thiol-Michael addition reaction exploiting AEMA linker on MAHA to obtain ELHA polysaccharide **3**. The synthetic route was chosen in order to perform a chemoselective strategy avoiding the unwanted reactions with the functionalized side chains of aminoacid residues. The conjugation reaction was conducted in H_2O, at pH = 8.9 in the presence of (tris(2-carboxyethyl)phosphine hydrochloride) TCEP·HCl at the same time as nucleophilic catalyst[30] and disulfide bond reducing agent.[31]

The ^{1}H NMR spectrum (Figure 1, blue) of **3** showed the disappearance of methacrylate signals at δ_{DSS} = 1.91, 5.73, and 6.14 ppm, that is in agreement with the quantitative coupling of peptide with methacrylate pending moiety. Moreover, the appearance of peptide side chain signals: δ_{DSS} = 7.16 ppm and δ_{DSS} = 6.83 ppm, δ_{DSS} = 1.54–1.30 ppm, δ_{DSS} = 0.91, and δ_{DSS} = 0.86 ppm assigned to aromatic protons of tyrosine, –CH_3 of alanine and leucine residues, respectively, confirmed the occurred reaction.

The degree of conjugation of peptide to HA is functional to preserve the biological activity of HA. Wound healing is regulated by HA-binding receptors, as the transmembrane protein CD44,[32] which interaction occurs mainly through the carboxylate group of GlcA, *N*-acetyl group of GlcNAc, and CD44 HA-binding domain.[33] Recent studies confirm that a moderate functionalization of polysaccharide backbone is fundamental to retain CD44 binding, that is otherwise altered in the case of higher degree of modification.[34]

ATR-FTIR analysis

The product's characterization was carried out by ATR-FTIR that allowed the assignment of specific functional groups in the spectra of HA, MAHA, EL and ELHA (Figure 2). HA spectrum (black curve) shows a broad band in 3500–3000 cm^{-1} region as expected for carbohydrate O–H stretching, as well as, amide I (orange star) and amide II (green star) bands of acetamido groups are observed at ~1605 and ~1550 cm^{-1}, respectively.

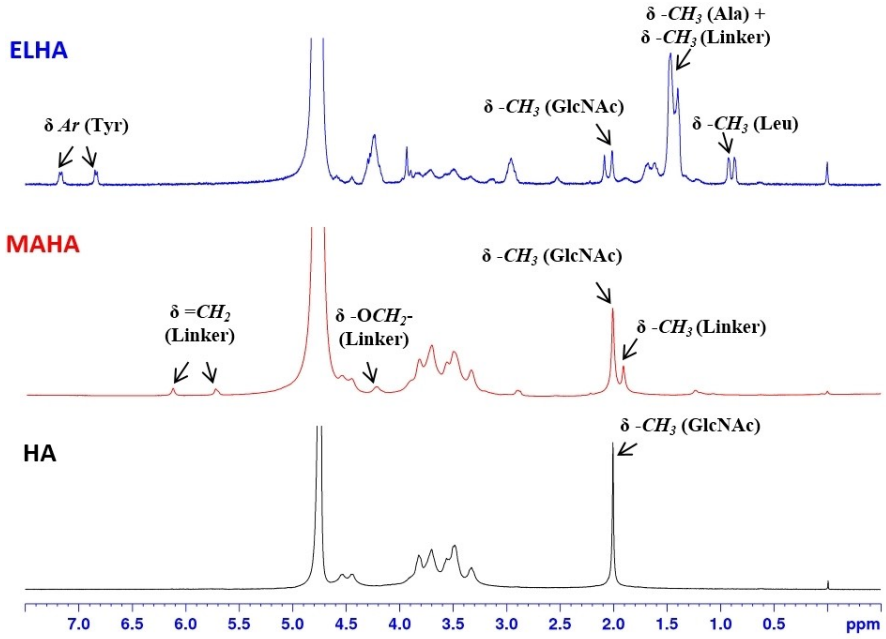

Figure 1. ^{1}H NMR spectra of HA (black), polysaccharide **2** (MAHA, red), and polysaccharide **3**, (ELHA, blue) (400 MHz, D_2O, 298 K).

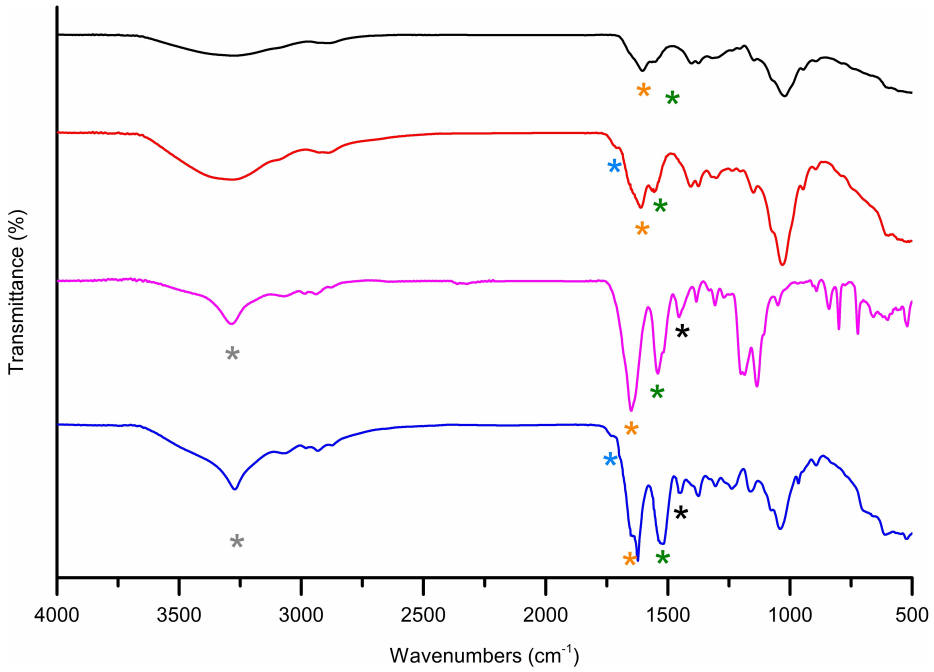

Figure 2. ATR spectra of HA (black), polysaccharide **2** (MAHA, red), peptide **1** (EL, purple), and polysaccharide **3**, (ELHA, blue). N–H stretching vibration band (gray star), ester C=O stretching vibration (blue star), amide C=O stretching vibration (orange star), amide C–N stretching vibration (green star), C-H_3 bending vibration (black star).

Polysaccharide **2** spectrum (MAHA, red curve) shows the presence of a band at ~1711 cm^{-1} (blue star) associated to unsaturated ester C=O stretching vibration.

Moreover, peptide coupling to methacrylated hyaluronic acid was confirmed by polysaccharide **3** spectrum (ELHA, blue curve). The appearance of the N–H stretching band (gray star) is assigned to the peptide amide bond. It appears in the region hosting the broad band at ~3281 cm^{-1} assigned to the O–H stretching of HA present also in polysaccharide **2** (red curve). Furthermore, the upshift of band associated to ester C=O stretching vibration from ~1711 to ~1733 cm^{-1} (blue star) moving from polysaccharide **2** to polysaccharide **3** is due to the loss of conjugated π system. Finally, amide I band at 1650 cm^{-1} (orange star) and amide II band at 1525 cm^{-1} (green star) derived from amide C=O stretching vibration, amide C–N stretching coupled to N–H bending vibrations, respectively, confirms the occurred coupling reaction. The Amide I band is sensitive to the secondary structure of the peptide.[35] Accordingly, the band at 1650 cm^{-1} is ascribed to peptide in alpha-helical conformation.[36] Analogous finding could be deduced from the band at ~1450 cm^{-1} (black star) associated to the asymmetric C-H_3 bending vibration of alanine residues, which are present in peptide **1** spectrum (purple curve) and absent in HA and polysaccharide **2** curves.

Circular dichroism

In order to have useful insights on the conformation of the peptide before and after conjugation to methacrylated polysaccharide, CD analysis is carried out in phosphate-buffered solution (PBS), pH = 7.4, as a function of the temperature. The comparison is realized among CD spectra recorded on peptide **1**, HA, and derivative **3**.

In PBS solution the CD spectrum of peptide **1** (Figure 3A) shows at 273 K a strong positive band centred at 192 nm and a negative band at 206 nm, both of them associated to π–π* transition of peptide bond chromophore. The negative band at 222 nm due to n-π* transition is also present in the spectrum. These spectral features are typical of an α-helix conformation confirming ATR-FTIR results.[25a,c] The increase of temperature to 298 and 310 K induces the gradual reduction in intensity of the bands, together with a slight blue-shift of the band at 206 nm suggesting the progressive destabilization of α-helix conformation because of the increase of random coil contribution. CD spectrum of HA in PBS solution (Figure 3B) shows, at 273 K, a strong negative band at 210 nm assigned to n-π* transitions of GlcNAc amide chromophore.[37] By increasing temperature from 298 to 310 K a gradual reduction in intensity of bands is observed. Hydroxyl, carboxyl and acetamido groups on HA backbone are responsible for hydrogen bonds interaction, which are affected by the temperature. A possible explanation of the CD spectral trend could be that the increase of the temperature induced the breaking of hydrogen bonds.

After bioconjugation, the obtained polysaccharide **3** showed CD spectra reported in Figure 3C. At 273 K the bands centred at 192 nm and 206 nm associated to π–π* transition of peptide bond chromophore, and the band at 222 nm due to n–π* transitions are visible. They gradually decrease on increasing the temperature. These spectral findings suggest the persis-

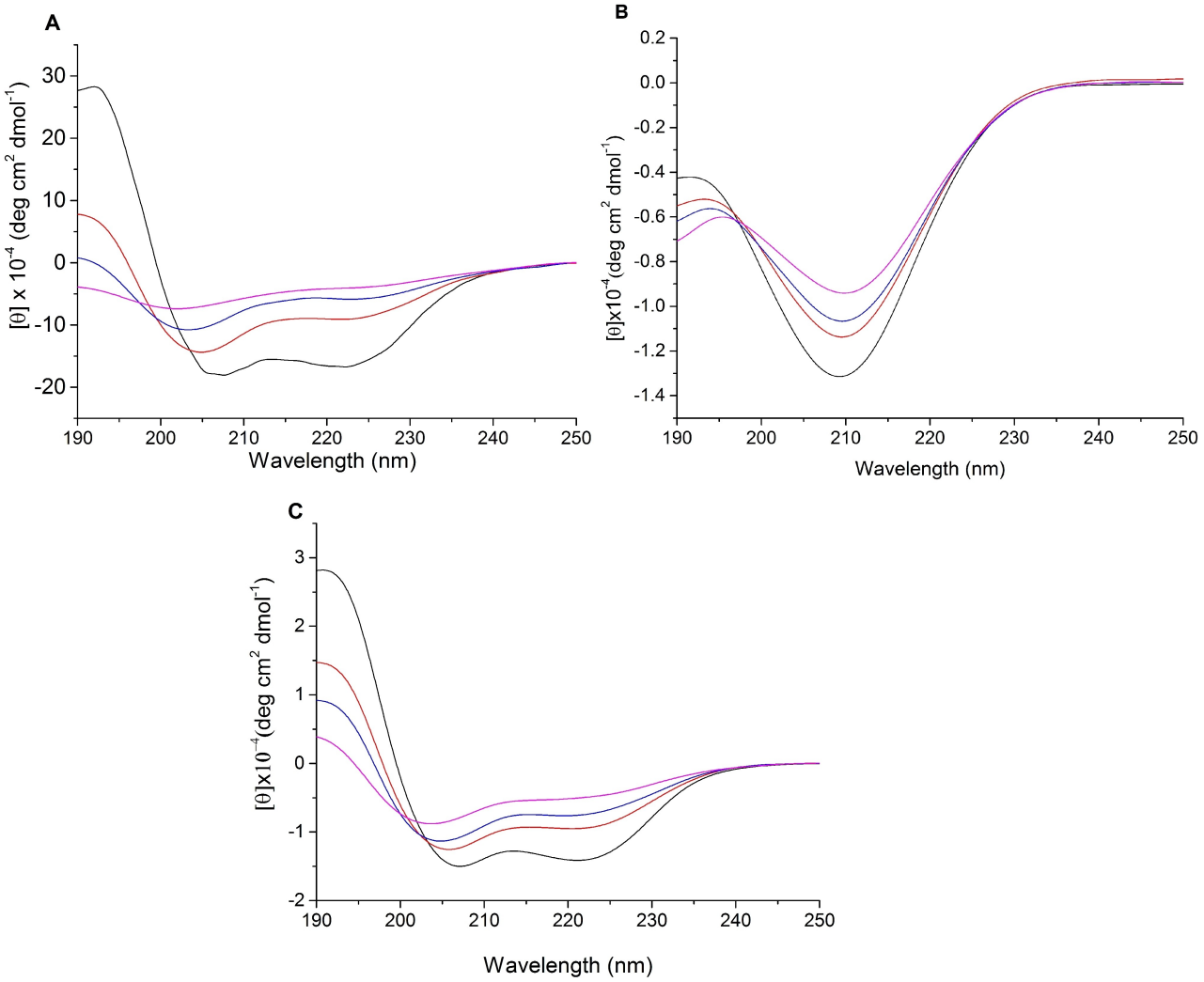

Figure 3. Temperature-dependent CD spectra in PBS solution of: A) peptide **1**, B) HA, C) polysaccharide **3**, (ELHA) recorded at 273 K (black), 298 K (red), 310 K (blue), 333 K (purple).

tence of α-helix conformation. Therefore, we can conclude that contribution of α-helix conformation of the conjugated peptide is still dominant, even though only 18% of disaccharide repeating units have been functionalized. The conservation of α-helix conformation in the bioconjugated derivative **3** is essential for the peptide bioactivity.[38]

Electrospinning

Recently, electrospinning has gained great diffusion as a tool to produce nanofibrous scaffolds useful in wound dressings.[39] Our aim is to produce electrospun scaffolds made of biodegradable and bioactive polymers. HA, derivatives **2** and **3** were blended with PDLLA polymer and electrospun as described in Table 1.

Table 1. Scaffolds composition and electrospinning process parameters.

Abbreviation[a]	Composition	Polymer weight ratio [w/w]	Final concentration % [w/V]	Electrospinning process parameters			
				V [kV]	N [G]	D [cm]	F [mL/h]
P	PDLLA	–	12.00%	19	18	19	0.5
HP	HA/PDLLA	1:50	12.24%	19	18	19	0.5
MHP	MAHA/PDLLA	1:50	12.24%	19	18	19	0.5
EHP	ELHA/PDLLA	1:50	12.24%	19	18	19	0.5

[a] P: (poly-lactic acid), HP: (hyaluronic acid/poly-lactic acid), MHP: (methacrylated hyaluronic acid/poly-lactic acid), EHP: (elastin-conjugated hyaluronic acid/poly-lactic acid).

HFP, known for its low nucleophilicity and strong hydrogen bond-donating ability,[40] was chosen as solvent because of its ability to solubilize both PDLLA polymer and EI peptides.[10b] Herein, HFP was mixed together with H_2O, to dissolve HA, derivatives **2** and **3**. HP (HA/PDLLA), MHP (MAHA/PDLLA) and EHP (ELHA/PDLLA) blends were prepared by dissolving in 80% HFP aqueous solution either HA, MAHA or ELHA and PDLLA to a final concentration of 0.24% and 12.0% (w/V), respectively. In the same way P scaffold, containing pristine PDLLA, was prepared by dissolving the polymer in 80% HFP aqueous solution to a final concentration of 12.0% (w/V). The electrospinning parameters were tuned in order to assure the process stability. The final results were membranes showing a uniform structure at the macroscopic level.

Moreover, the embedding of polysaccharide derivatives in the hybrid scaffolds was investigated by ATR-FTIR. Concerning derivative **2**, the limited quantity of MAHA in MHP scaffold did not allow a clear detection (data not shown). ATR-FTIR spectrum of EHP scaffold containing derivative **3** is shown in Figure S5 where at ~3281 cm^{-1} the band associated to the N–H stretching vibration of peptide bond (filled gray circle), and at ~1751 cm^{-1} the band associated to PDLLA ester C=O stretching vibration (filled yellow circle) are visible. An additional evidence of the glycoconjugate incorporation in the EHP membrane is the presence of amide I band at 1650 cm-1 (filled green circle) and amide II band at ~1540 cm^{-1} (filled blue circle) assigned to the peptide in alpha-helical conformation.

The morphology of the scaffolds was investigated by scanning electron microscopy (SEM), with particular attention to the assessment of any defect (beads), to the fibers' orientation, and diameter distribution. The SEM image of the electrospun P scaffold (Figure 4A) showed a three-dimensional microstructure enriched with interconnected pores, and bead-on-string morphology, that typically arises when the charge repulsion and viscous forces are surmounted by surface tension of the liquid.[41]

Charge density is mainly influenced by the applied voltage, whereas viscosity and surface tension depend on the polymer and the solvent used for preparing the solution to electrospun. In comparison to pure HFP solution, the presence of H_2O increases surface tension leading to beads formation.[42] HP, MHP and EHP scaffolds displayed, indeed, fibers with a linear trend, without beads, suggesting an effective dispersion of the polysaccharides in the mixture (Figure 4B–D). Moreover, for EHP scaffold the fibers appeared slightly curled. A possible interpretation could be that the solution viscosity increased with the addition of MAHA and ELHA, counterbalancing the negative effect exerted by surface tension on morphology, and enabling the formation of fibers without beads.

The average diameters of fibers as function of frequency (Figures S6 A–D) showed a normal distribution around a mean value of 447.65 ± 121.09, 416.61 ± 34.15, 476.99 ± 40.37, and 343.51 ± 40.07 nm for P, HP, MHP, and EHP electrospun scaffolds, respectively, as reported in Table 2.

For evaluating differences in fibers diameter, statistical analyses using the one-way Analysis of Variance (ANOVA) method and Tukey's Test were conducted. Between P and HP, as well as, P and MHP membranes, no significant difference was observed, whereas a statistical increase was found by comparison of HP and MHP membranes (Figure 5) with $p^* \leq 0.01$ (from 416.61 ± 34.15 to 476.99 ± 40.37 nm). This phenomenon could be associated with the slight increase of polysaccharide molecular weight after methacrylate introduction. Concerning

Table 2. Scaffolds morphology.

Scaffold[a]	Average fiber diameter[b] [nm]
P	447.65 ± 121.09
HP	416.61 ± 34.15
MHP	476.99 ± 40.37
EHP	343.51 ± 40.07

[a] P: (poly-lactic acid), HP: (hyaluronic acid/poly-lactic acid), MHP: (methacrylated hyaluronic acid/poly-lactic acid), EHP: (elastin-conjugated hyaluronic acid/poly-lactic acid). [b] Mean value ± standard deviation (n > 100 from three different images).

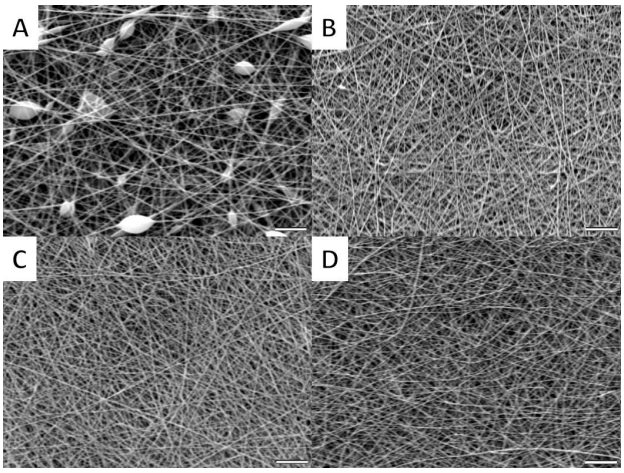

Figure 4. SEM images of electrospun scaffolds. P (A), HP (B), MHP (C), and EHP (D); (bar: 20 μm).

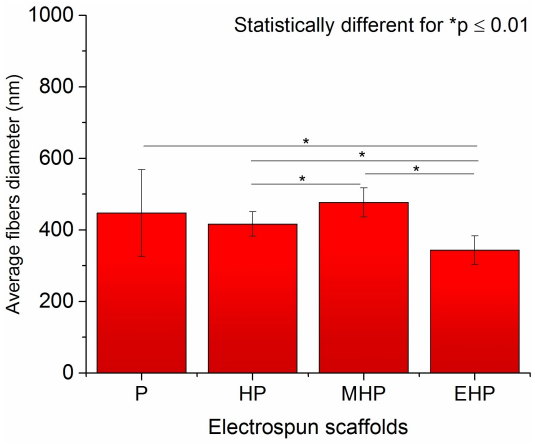

Figure 5. Histogram of average fibers diameter for P, HP, MHP, and EHP electrospun scaffolds.

EHP scaffold, the presence of ELHA glycoconjugate induced a significant reduction of average fibers diameter with $p^* \leq 0.01$ respect to all other scaffolds (Table 2).

This finding could be ascribed either to the applied voltage or to solution physical properties. In our case, P, HP, MHP, and EHP membranes have been electrospun by using the same process parameters, therefore the statistical decrease in nanofibers diameter could be attributed to the acidic pH of HFP/H_2O solution, giving rise to positively charged ε-amine of Lys residues in the polysaccharide **3**. The final effect is the increase of solution conductivity.

Considering that the average fibers diameter of the obtained membranes might be suitable for biomedical applications as reported by Kenar and co-workers,[43] the defect-free interconnected nanostructures of HP, MHP and EHP scaffolds well mimics ECM three-dimensional network, as well as enable oxygen and vapor permeation. These features are fundamental for optimal wound dressings design.

Conclusion

In the present work, we reported the semi-synthesis of ELHA glycoconjugate obtained by coupling elastin-derived peptide with methacrylated hyaluronic acid. Conformational studies confirmed that the conjugated elastin peptide preserves the α-helix conformation, crucial for its biological activity, even in the electrospun scaffold. This result renders ELHA appealing in wound healing applications. Therefore, a set of bio-inspired electrospun scaffolds composed of HA, MAHA, ELHA, and PDLLA, has been produced and investigated at the microscopic level. The addition of polysaccharide ELHA enabled the production of interconnected defect-free structures with thin fibres.

To the best of our knowledge, this is the first work reporting the electrospinning of bio-inspired scaffolds obtained by blending polymers with semi-synthetic elastin-peptide conjugated HA derivative, which would open a route towards the investigation of structure-activity relationship of semi-synthetic glycoconjugates embedded in polymer nanofibers. Work to this aim is currently in progress and will be published in due time.

Experimental Section

Materials: Commercial-grade reagents and solvents were used without further purification, except where otherwise indicated. The term "pure H_2O" refers to water purified by a Millipore Milli-Q Gradient system. Hyaluronic acid sodium salt (MW = 186 KDa) medical device grade was a generous gift of Altergon Italia SrL "(Morra de Sanctis, AV, Italy)". 9-Fmoc-amino-xanthen-3-yl-oxymethyl-copoly(styrene – 1% DVB)) (100–200 mesh, theoretical loading = 0.34 mmol/g, Rink amide) resin was purchased from Novabiochem®.

1,2-Ethanedithiol (≥98.0%, EDT), 2-Aminoethylmethacrylate hydrochloride (≥98.0%, AEMA), dichloromethane (≥99.8%, CH_2Cl_2), diethyl ether (99.5%, Et_2O), dimethyl sulfoxide-d6 (99.0%, DMSO-d_6), sodium chloride (≥99.0%, NaCl), sodium hydroxide pellets (≥98.0%, NaOH), sodium phosphate monobasic (>99.0%, NaH_2PO_4), trifluoroacetic acid (≥99.0%, TFA), triisopropylsilane (≥98.0%, TIS), and 3-(Trimethylsilyl)propionic-2,2,3,3-d_4 acid sodium salt (98.0%, DSS) were purchased from Sigma Aldrich.

N-(9-Fluorenylmethoxycarbonyl)-L-alanine (Fmoc-Ala-OH), *N*-(9-Fluorenylmethoxycarbonyl)-glicine (Fmoc-Gly-OH), *N*-(9-Fluorenylmethoxycarbonyl)-S-*tert*-butyl-L-cysteine (Fmoc-Cys(tBu)-OH), *N*-(9-Fluorenylmethoxycarbonyl)-L-leucine (Fmoc-Leu-OH), *N*-(9-Fluorenylmethoxycarbonyl)-6-(*tert*-butoxycarbonyl)-L-lysine (Fmoc-Lys(Boc)-OH), *N*-(9-Fluorenylmethoxycarbonyl)-*O*-*tert*-butyl-L-tyrosine (Fmoc-Tyr(tBu)-OH), and *N,N,N′,N′*-Tetramethyl-*O*-(1H-benzotriazol-1-yl)-uronium hexafluorophosphate (HBTU) were purchased from INBIOS.

N,N-Diisopropylethylamine (≥99%, DIPEA), and *N,N*-Dimethylformamide (>99.9%, DMF), were purchased from ROMIL. 1-Hydroxybenzotriazole hydrate (≥98%, HOBt), and acetic anhydride (≥99%,Ac_2O) were furnished by Fluka. *N*-(3-(Dimethylamino)propyl)-*N′*-ethylcarbodiimide hydrochloride (EDC·HCl) was purchased from Iris Biotech GmbH, and *N*-Hydroxysulfosuccinimide sodium salt (>98%, Sulfo-NHS) was purchased from TCI Chemicals. Acetonitrile (≥99.9%) HiPerSolv CHROMANORM® was purchased from VWR. Tris(2-carboxyethyl)phosphine hydrochloride (TCEP·HCl) was purchased from ThermoFisher Scientific.

General Methods: Peptide synthesis was performed on a Protein Technologies, Inc Tribute® automatic synthesizer. Centrifugations were performed with a LaborTechnik GmbH Hermle Centrifuge instrument at 4 °C (7000 rpm, 30 min). Dialyses were conducted on Slide-A-Lyzer™ Dialysis Cassette G2 2.0 kDa cut-off membranes at 25 °C for MAHA and 3.5 kDa for ELHA. Freeze-drying was performed with a Christ Alpha 1–4 LD plus freeze-dryer.

High-Performance Liquid Chromatography (HPLC): Peptide analysis and purification were conducted by reverse-phase HPLC respectively on a Phenomenex Jupiter Proteo 90 Å C12 analytical column (250×4.60 mm) and on a Phenomenex Jupiter Proteo 90 Å C12 semi-preparative column (250×10 mm). The crude peptide was dissolved in H_2O (0.1% TFA) (0.5 mg/mL) and eluted in H_2O (0.1% TFA) - CH_3CN (0.1% TFA) in a 95:5 ratio, respectively, used as mobile phases in the binary gradient.

Matrix-Assisted Laser Desorption Ionization Time of Flight Mass (MALDI-TOF) Spectrometry: Purity of peptide was assessed by High Resolution Mass Spectrometry (HRMS) utilizing MALDI-TOF mass spectrometry by CEINGE (Naples, Italy).

Circular Dichroism (CD) Spectroscopy: CD spectra were recorded on a JASCO J-815 Spectropolarimeter, equipped with a HAAKE temperature controller. Samples were dissolved at a concentration of 0.1 mg/mL, 0.5 mg/mL, and 0.25 mg/mL in pH 7.4 PBS 10 mM solution respectively for peptide **1** (EL), HA, polysaccharide **3** (ELHA) and loaded into cylindrical quartz cells with 1 mm pathlength. Spectra were acquired in a wavelength range of 190–250 nm at 273, 298, 310, and 333 K, with a scan speed of 20 nm min^{-1} and a band width of 1 nm. CD spectra represented the average of 16 scans. The CD spectra were processed using the JASCO Spectral analysis software. After background subtraction, a FFT filtering algorithm was applied for smoothing, and data were expressed as molar ellipticity [Θ] deg cm^2 $dmol^{-1}$. For HA and ELHA data were expressed as molar ellipticity [Θ] deg cm^2 $dmol^{-1}$ of disaccharide repeating unit. CD spectra of peptide were carried out in presence of reducing agent 1 mM tris(2-carboxyethyl)phosphine hydrochloride (TCEP).

Nuclear magnetic resonance (NMR) Spectroscopy: NMR spectra were recorded on 500 MHz (^{1}H: 500 MHz, ^{13}C:125 MHz) and 400 MHz (^{1}H: 400 MHz, ^{13}C: 100 MHz) Varian Inova instruments in D_2O (DSS 0.1 mM as internal standard, $\delta_H = 0$ ppm, $\delta_C = 0$ ppm). The

degree of substitution (DS) of **2** and **3** is attributed to disaccharide repeating units.

Attenuated Total Reflectance (ATR) Spectroscopy: ATR spectra were carried out on J-460 (Jasco Europe Srl) equipped with ATR accessory, Smart Orbit with a type II A diamond crystal, refractive index 2.4, with a KBr beam splitter and a MCT/B detector. Spectra were acquired in the region from 4000 to 450 cm^{-1} with a spectral resolution of 2 cm^{-1} and 256 scans. Background spectra were recorded each time and then subtracted from the sample spectra.

Scanning Electron Microscopy (SEM): SEM images were acquired with a voltage of 20 kV and different magnifications, after gold sputter-coating on a Philips, FEI ESEM XL30 instrument. The diameter of the fibers was evaluated using ImageJ software supplied with the DiameterJ plug-in ($n > 100$).

Synthesis of Ac-CAAAAAAAAAAKAAKYGAAGL-NH_2 peptide 1: SPPS synthesis was accomplished as described in Supporting Information.

Synthesis of derivative 2: Sodium hyaluronate (98.40 mg, 0.245 mmol) was suspended in pure H_2O (15.0 mL) and stirred at room temperature up to complete dissolution, then treated with a 49.6 mM EDC (10.0 mL, 0.486 mmol) and 24.8 mM NHS (10.0 mL, 0.246 mmol) solution. After five minutes a 122.2 mM AEMA (4.0 mL, 0.248 mmol) was added to the reaction mixture resulting in a molar ratio of 1:2:2 (NHS:EDC:AEMA), obtaining a yellowish suspension. Few drops of freshly prepared 1.0 M NaOH solution were then added to adjust pH to 6.5, and stirring was continued overnight. After ~20 h, the crude was neutralized by HCl 1.0 M and centrifuged, the supernatant was dialyzed against NaCl 150 mM solution for 2 days, and against H_2O for further 2 days. The subsequent freeze-drying yielded a white solid (101.17 mg, yield: 98%). ^{1}H NMR (400 MHz, D_2O): $\delta_{DSS} = 6.13$ (1H, CH_a Linker), 5.73 (1H, CH_b Linker), 4.54 (1H, H-1 GlcNAc), 4.44 (1H, H-1 GlcA), 4.22 (2H, CH_{2a} Linker), 3.83-3.33 (12 H), 2.01 (3H, CH_3 NHAc), 1.91 (3H, CH_3 Linker).

Synthesis of derivative 3: Polysaccharide **2** (9.81 mg, 0.023 mmol) was suspended in pure H_2O (1.5 mL) and stirred at room temperature up to complete dissolution. Simultaneously, peptide **1** (52.25 mg, 0.028 mmol) and TCEP·HCl (11.99 mg, 0.042 mmol) were dissolved in pure H_2O (2.0 mL) at room temperature. After five minutes this solution was added to **2** and the pH was adjusted to 8.9 with freshly prepared 1.0 M NaOH solution. After 48 h at room temperature the mixture was neutralized with HCl 0.1 M solution and dialyzed against NaCl 150 mM solution for 2 days, and against H2O for further 2 days. The subsequent freeze-drying yielded a white solid (10.96 mg, yield: 67%). ^{1}H NMR (400 MHz, D_2O): $\delta_{DSS} =$ 7.19 (2H, H–Ar Tyr), 6.85 (2H, H–Ar Tyr), 4.58 (1H, H-1 GlcNAc), 4.44 (1H, H-1 GlcA), 4.24 (17H, H_α Ala, Leu, Lys), 3.93 (2H, H_α Gly), 3.89–3.33 (14H), 3.13 (1H, H_β Cys), 3.04–2.86 (H_β Tyr, H_β Cys, H_ε Lys, CH Linker), 2.16–2.01 (6H, CH_3 NHAc GlcNAc, CH_3 NHAc Cys), 1.88 (1H, H_β Lys), 1.77-1.27 (56H, $H_\alpha + H_\beta$ Leu. $H_\beta + H_\gamma + H_\delta$ Lys, CH_3 Ala, CH_3 Linker), 0.89 (6H, CH_3 Leu).

Electrospinning: Polymer solution in the ratio percentages listed in Table 1 were prepared as follows: polysaccharide **2** or polysaccharide **3** (2.9 mg) were dissolved in 80% HFP aqueous solution (1.00 mL), then PDLLA (120 mg) was added and the mixture was kept under magnetic stirring overnight at room temperature. In the case of pure polyester solution, PDLLA (120 mg) was dissolved in 80% HFP aqueous solution (1.00 mL) and the solution was kept under magnetic stirring overnight at RT. The polymer mixtures were loaded into a 10 mL glass syringe with an 18 G stainless-steel needle and then electrospun at 19 kV with a flow rate of 0.5 mL/h of the pump. The target was a round copper plate having 90 mm diameter coated with aluminum foils and the distance between the collector and the needle was set to 19 cm.

Acknowledgements

The authors thank Altergon SrL (Morra De Sanctis, AV, Italy) for hyaluronic acid supply and Mr. Alessandro Laurita (Microscopy Center, University of Basilicata, Potenza, Italy) for SEM images. The authors are grateful for the financial support by PON R&I 2014–2020 (cod: PON_ARS01_01081 and PON_AIM1852803 Linea 1) from MUR. Open Access funding provided by Università degli Studi della Basilicata within the CRUI-CARE Agreement.

Conflict of Interest

The authors declare no conflict of interest.

Data Availability Statement

The data that support the findings of this study are available from the corresponding author upon reasonable request.

Keywords: bioconjugation · circular dichroism · elastin peptides · electrospinning · hyaluronic acid

[1] a) R. P. Mecham, *Curr. Protoc. Cell. Biol.* **2012**, *57*, 10.11.11-10.11.16; b) N. K. Karamanos, A. D. Theocharis, Z. Piperigkou, D. Manou, A. Passi, S. S. Skandalis, D. H. Vynios, V. Orian-Rousseau, S. Ricard-Blum, C. E. H. Schmelzer, L. Duca, M. Durbeej, N. A. Afratis, L. Troeberg, M. Franchi, V. Masola, M. Onisto, *FEBS J.* **2021**, *288*, 6850–6912.
[2] I. M. Braverman, E. Fonferko, *J. Invest. Dermatol.* **1982**, *78*, 434–443.
[3] M. Vila, A. Garcia, A. Girotti, M. Alonso, J. C. Rodriguez-Cabello, A. Gonzalez-Vazquez, J. A. Planell, E. Engel, J. Bujan, N. Garcia-Honduvilla, M. Vallet-Regi, *Acta Biomater.* **2016**, *45*, 349–356.
[4] A. Keirouz, M. Chung, J. Kwon, G. Fortunato, N. Radacsi, *Wiley Interdiscip. Rev. Nanomed. Nanobiotechnol.* **2020**, *12*, e1626.
[5] a) C. Gao, L. Zhang, J. Wang, M. Jin, Q. Tang, Z. Chen, Y. Cheng, R. Yang, G. Zhao, *J. Mater. Chem. B* **2021**, *9*, 3106–3130; b) A. Memic, T. Abudula, H. S. Mohammed, K. Joshi Navare, T. Colombani, S. A. Bencherif, *ACS Appl. Bio. Mater.* **2019**, *2*, 952–969.
[6] a) G. Piccirillo, M. V. Ditaranto, N. F. S. Feuerer, D. A. Carvajal Berrio, E. M. Brauchle, A. Pepe, B. Bochicchio, K. Schenke-Layland, S. Hinderer, *J. Mater. Chem. B* **2018**, *6*, 6399–6412; b) B. Bochicchio, K. Barbaro, A. De Bonis, J. V. Rau, A. Pepe, *J. Biomed. Mater. Res. Part A* **2020**, *108*, 1064–1076; c) C. Ru, F. Wang, M. Pang, L. Sun, R. Chen, Y. Sun, *ACS Appl. Mater. Interfaces* **2015**, *7*, 10872–10877; d) A. Toncheva, M. Spasova, D. Paneva, N. Manolova, I. Rashkov, *Int. J. Polym. Mater. Polym. Biomater.* **2014**, *63*, 657–671.
[7] A. Chanda, J. Adhikari, A. Ghosh, S. R. Chowdhury, S. Thomas, P. Datta, P. Saha, *Int. J. Biol. Macromol.* **2018**, *116*, 774–785.
[8] X. Liu, T. Lin, J. Fang, G. Yao, H. Zhao, M. Dodson, X. Wang, *J. Biomed. Mater. Res. Part A* **2010**, *94*, 499–508.
[9] a) R. Machado, A. da Costa, V. Sencadas, C. Garcia-Arevalo, C. M. Costa, J. Padrao, A. Gomes, S. Lanceros-Mendez, J. C. Rodriguez-Cabello, M. Casal, *Biomed. Mater.* **2013**, *8*, 065009; b) M. Li, M. J. Mondrinos, X. Chen, M. R. Gandhi, F. K. Ko, P. I. Lelkes, *J. Biomed. Mater. Res. Part A* **2006**, *79*, 963–973; c) L. Buttafoco, N. G. Kolkman, P. Engbers-Buijtenhuijs, A. A. Poot, P. J. Dijkstra, I. Vermes, J. Feijen, *Biomaterials* **2006**, *27*, 724–734; d) J. Han, P. Lazarovici, C. Pomerantz, X. Chen, Y. Wei, P. I. Lelkes, *Biomacromolecules* **2011**, *12*, 399–408.
[10] a) N. Ciarfaglia, A. Laezza, L. Lods, A. Lonjon, J. Dandurand, A. Pepe, B. Bochicchio, *J. Appl. Polym. Sci.* **2021**, *138*, 51313; b) N. Ciarfaglia, A.

Pepe, G. Piccirillo, A. Laezza, R. Daum, K. Schenke-Layland, B. Bochicchio, *ACS Appl. Polym. Mater.* **2020**, *2*, 4836–4847.
[11] H. Wang, D. Zhu, A. Paul, L. Cai, A. Enejder, F. Yang, S. C. Heilshorn, *Adv. Funct. Mater.* **2017**, *27*.
[12] V. Hascall, J. D. Esko in *Essentials of Glycobiology*, (Eds.: A. Varki, R. D. Cummings, J. D. Esko, H. H. Freeze, P. Stanley, C. R. Bertozzi, G. W. Hart, M. E. Etzler), The Consortium of Glycobiology Editors, La Jolla, California., Cold Spring Harbor NY, **2009, pp. 219-228**.
[13] a) J. S. Frenkel, *Int. Wound J.* **2014**, *11*, 159–163; b) W. Y. J. Chen in *Functions of Hyaluranon in wound repair, Vol.* Eds.: J. F. Kennedy, G. O. Phillips, P. A. Williams), Woodhead Publishing, **2002**, pp. 147–156.
[14] J. Voigt, V. R. Driver, *Wound Repair Regen.* **2012**, *20*, 317–331.
[15] a) M. F. P. Graça, S. P. Miguel, C. S. D. Cabral, I. J. Correia, *Carbohydr. Polym.* **2020**, *241*, 116364; b) B. Ebrahimi-Hosseinzadeh, M. Pedram, A. Hatamian-Zarmi, S. Salahshour-Kordestani, M. Rasti, Z. B. Mokhtari-Hosseini, M. Mir-Derikvand, *Fibers Polym.* **2016**, *17*, 820–826.
[16] G. Piccirillo, N. Feuerer, D. A. Carvajal Berrio, S. L. Layland, S. Reimer Hinderer, B. Bochicchio, K. Schenke-Layland, *Tissue Eng., Part C: Methods* **2021**, *27*, 589–604.
[17] G. Piccirillo, B. Bochicchio, A. Pepe, K. Schenke-Layland, S. Hinderer, *Acta Biomater.* **2017**, *52*, 187–196.
[18] F. S. Palumbo, G. Pitarresi, D. Mandracchia, G. Tripodo, G. Giammona, *Carbohydr. Polym.* **2006**, *66*, 379–385.
[19] D. Zhu, H. Wang, P. Trinh, S. C. Heilshorn, F. Yang, *Biomaterials* **2017**, *127*, 132–140.
[20] a) C. C. L. Schuurmans, M. Mihajlovic, C. Hiemstra, K. Ito, W. E. Hennink, T. Vermonden, *Biomaterials* **2021**, *268*, 120602; b) F. Xing, C. Zhou, D. Hui, C. Du, L. Wu, L. Wang, W. Wang, X. Pu, L. Gu, L. Liu, Z. Xiang, X. Zhang, *Nanotechnol. Rev.* **2020**, *9*, 1059–1079; c) E. Shirzaei Sani, R. Portillo-Lara, A. Spencer, W. Yu, B. M. Geilich, I. Noshadi, T. J. Webster, N. Annabi, *ACS Biomater. Sci. Eng.* **2018**, *4*, 2528–2540; d) M. H. M. Oudshoorn, R. Rissmann, J. A. Bouwstra, W. E. Hennink, *Polymer* **2007**, *48*, 1915–1920; e) J. A. Burdick, C. Chung, X. Jia, M. A. Randolph, R. Langer, *Biomacromolecules* **2005**, *6*, 386–391.
[21] P. Bulpitt, D. Aeschlimann, *J. Biomed. Mater. Res.* **1999**, *47*, 152–169.
[22] G. Piccirillo, A. Pepe, E. Bedini, B. Bochicchio, *Chem. Eur. J.* **2017**, *23*, 2648–2659.
[23] C. E. Hoyle, C. N. Bowman, *Angew. Chem. Int. Ed. Engl.* **2010**, *49*, 1540–1573.
[24] P. Lee, G. C. Yeo, A. S. Weiss, *FEBS J.* **2017**, *284*, 2216–2230.
[25] a) S. E. Reichheld, L. D. Muiznieks, R. Stahl, K. Simonetti, S. Sharpe, F. W. Keeley, *J. Biol. Chem.* **2014**, *289*, 10057–10068; b) B. Bochicchio, A. Pepe, *Chirality* **2011**, *23*, 694–702; c) A. M. Tamburro, M. Lorusso, N. Ibris, A. Pepe, B. Bochicchio, *Chirality* **2010**, *22 Suppl 1*, E56–66; d) A. M. Tamburro, A. Pepe, B. Bochicchio, *Biochemistry* **2006**, *45*, 9518–9530.
[26] a) Y. M. Angell, J. Alsina, F. Albericio, G. Barany, *J. Pept. Res.* **2002**, *60*, 292–299; b) Y. Han, F. Albericio, G. Barany, *J. Org. Chem.* **1997**, *62*, 4307–4312.
[27] A. El-Faham, F. Albericio, *Chem. Rev.* **2011**, *111*, 6557–6602.
[28] T. Borke, F. M. Winnik, H. Tenhu, S. Hietala, *Carbohydr. Polym.* **2015**, *116*, 42–50.
[29] E. Bedini, A. Laezza, A. Iadonisi, *Eur. J. Org. Chem.* **2016**, *2016*, 3018–3042.
[30] G.-Z. Li, R. K. Randev, A. H. Soeriyadi, G. Rees, C. Boyer, Z. Tong, T. P. Davis, C. R. Becer, D. M. Haddleton, *Polym. Chem.* **2010**, *1*, 1196–1204.
[31] J. A. Burns, J. C. Butler, J. Moran, G. M. Whitesides, *J. Org. Chem.* **1991**, *56*, 2648–2650.
[32] K. L. Aya, R. Stern, *Wound Repair Regen.* **2014**, *22*, 579–593.
[33] S. Banerji, A. J. Wright, M. Noble, D. J. Mahoney, I. D. Campbell, A. J. Day, D. G. Jackson, *Nat. Struct. Mol. Biol.* **2007**, *14*, 234–239.
[34] M. Y. Kwon, C. Wang, J. H. Galarraga, E. Pure, L. Han, J. A. Burdick, *Biomaterials* **2019**, *222*, 119451.
[35] a) S. Krimm, J. Bandekar, *Adv. Protein Chem.* **1986**, *38*, 181–364; b) W. K. Surewicz, H. H. Mantsch, D. Chapman, *Biochemistry* **1993**, *32*, 389–394.
[36] J. Kong, S. Yu, *Acta Biochim. Biophys. Sin.* **2007**, *39*, 549–559.
[37] a) L. A. Buffington, E. S. Pysh, B. Chakrabarti, E. A. Balazs, *J. Am. Chem. Soc.* **1977**, *99*, 1730–1734; b) A. L. Stone, *Biopolymers* **1971**, *10*, 739–751; c) A. L. Stone, *Biopolymers* **1969**, *7*, 173–187.
[38] B. Bochicchio, G. C. Yeo, P. Lee, D. Emul, A. Pepe, A. Laezza, N. Ciarfaglia, D. Quaglino, A. S. Weiss, *FEBS J.* **2021**, *288*, 4024–4038.
[39] Y. Q. Liu, T. Y. Li, Y. F. Han, F. J. Li, Y. Liu, *Curr. Opin. Biomed. Eng.* **2021**, *17*, 100247.
[40] I. Colomer, A. E. R. Chamberlain, M. B. Haughey, T. J. Donohoe, *Nat. Chem. Rev.* **2017**, *1*, 0088.
[41] G. R. Williams, B. T. Raimi-Abraham, C. J. Luo in *Nanofibres in Drug Delivery*, UCL Press, **2018**, pp. 24–59.
[42] H. Fong, I. Chun, D. H. Reneker, *Polymer* **1999**, *40*, 4585–4592.
[43] H. Kenar, C. Y. Ozdogan, C. Dumlu, E. Doger, G. T. Kose, V. Hasirci, *Mater. Sci. Eng. C* **2019**, *97*, 31–44.

Manuscript received: June 24, 2022
Accepted manuscript online: August 2, 2022
Version of record online: ■■, ■■■

RESEARCH ARTICLE

The persistence of α-helix conformation in a bioactive peptide after the conjugation with hyaluronic acid confirms thiol-ene chemistry as a successful strategy adopting mild conditions. The electrospun scaffolds showed the double advantage of an improved regularity of nanofiber pattern by hyaluronic acid addition and the presence of a bioactive peptide.

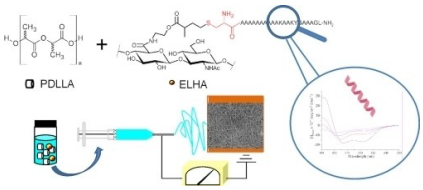

*Dr. A. Laezza, Prof. A. Pepe, Prof. B. Bochicchio**

1 – 10

Elastin-Hyaluronan Bioconjugate as Bioactive Component in Electrospun Scaffolds